Journal of Inflammation Research

Dovepress
Taylor & Francis Group

Open Access Full Text Article

ORIGINAL RESEARCH

Suxiao Jiuxin Pill Promotes Post-Myocardial Infarction Cardiac Repair by Enhancing Regulatory T Cell Function via the ST2L Signaling Pathway

Lusha Zhang[1–3,*], Ying Guo[1,*], Yuming Fan[1], Ting Liu[1], Tianyu Wang[1], Mengyao Li[1], Shaoxia Wang[1], Qi Yu[2], Hong Wang[1]

[1]School of Medical Technology, Tianjin University of Traditional Chinese Medicine, Tianjin, 301617, People's Republic of China; [2]Shaanxi Key Laboratory of Ischemic Cardiovascular Diseases and Institute of Basic and Translational Medicine, Xi'an Medical University, Xi'an, 710021, People's Republic of China; [3]Graduated School, Tianjin University of Traditional Chinese Medicine, Tianjin, 301617, People's Republic of China

*These authors contributed equally to this work

Correspondence: Hong Wang, School of Medical Technology, Tianjin University of Traditional Chinese Medicine, 10 Poyanghu Road, West Area, Tuanbo New Town, Jinghai District, Tianjin, 301617, People's Republic of China, Tel +8622595961171, Email wanghongsys@tjutcm.edu.cn; Qi Yu, Shaanxi Key Laboratory of Ischemic Cardiovascular Diseases and Institute of Basic and Translational Medicine, Xi'an Medical University, 1, Xinwang Road, Weiyang District, Xi 'An, 710021, People's Republic of China, Email qiyu6028@hotmail.com

Background: Clinical evidence suggests that extended treatment with Suxiao Jiuxin Pill (SJP) significantly reduces the recurrence rates of myocardial infarction (MI), primarily through its modulation of cardiac immune-fibrotic responses. Nonetheless, the precise molecular mechanisms underlying this effect remain to be fully elucidated.

Methods: Male C57BL/6J mice were randomly assigned to six groups: sham-operated control, MI + saline (vehicle control), MI + SJP (39, 78, and 156 mg/kg), and MI + dapagliflozin (1.5 mg/kg, positive control). Cardiac function and infarct size were assessed using echocardiography and Masson's trichrome staining. Serum levels of lactate dehydrogenase (LDH), creatine kinase (CK), and creatine kinase-MB (CK-MB) were measured with a Hitachi 7020 automatic biochemical analyzer, while cardiac troponin T (cTnT) levels were quantified via enzyme-linked immunosorbent assay (ELISA). Gene expression analysis was conducted using reverse transcription polymerase chain reaction (RT-PCR). Immune cell populations within the ischemic heart were analyzed through flow cytometry. Naïve $CD4^+$ T cells were isolated and differentiated into regulatory T cells (Tregs) to assess their immunosuppressive function.

Results: The administration of SJP treatment resulted in a significant reduction in infarct size and enhancement of cardiac function in mice with MI. Additionally, SJP modulated the immune profile of the infarcted myocardium by reducing neutrophil infiltration and increasing the presence of $CD4^+$ T cells and $CD206^+$ macrophages. Importantly, SJP markedly expanded the population of regulatory T cells (Tregs) and augmented their immunosuppressive capabilities, as evidenced by the upregulated expression of IL-10, Ctla-4, and Sparc. The cardioprotective effects of SJP were found to be dependent on Tregs, as their depletion negated the therapeutic benefits of SJP. Mechanistically, SJP facilitated Treg expansion within the infarcted myocardium by activating the ST2L/Foxp3 signaling pathway and restoring the balance between Treg and Th17 cytokines. In vitro analyses identified senkyunolide I and levistolide A as the predominant active compounds responsible for these effects.

Conclusion: This study elucidates the cardioprotective effects of SJP, which are mediated through the expansion of the Treg population and enhancement of their immunosuppressive function via activation of the ST2L/Foxp3 signaling pathway, with senkyunolide I and levistolide A identified as primary drivers behind the enhanced Treg function.

Keywords: Suxiao Jiuxin pill, myocardial infarction, ST2L, Treg

Introduction

Myocardial infarction (MI) remains a leading cause of global mortality.[1,2] While reperfusion therapies are life-saving, they fail to address the subsequent pathological inflammatory cascade and maladaptive remodeling that frequently culminate in heart failure.[3–6] This underscores a critical, unmet clinical need for therapies capable of effectively

https://doi.org/10.2147/JIR.S557620
Received: 1 August 2025
Accepted: 28 December 2025
Published: 6 January 2026

Graphical Abstract

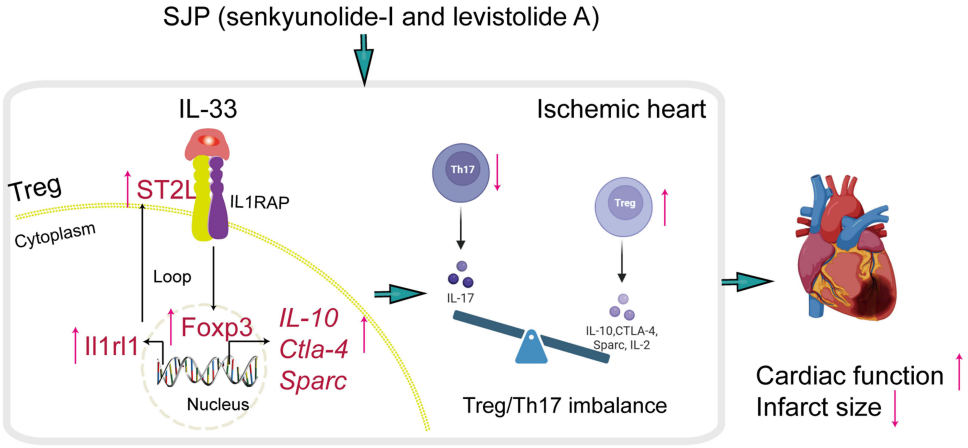

modulating the post-MI immune landscape to promote long-term cardiac repair. Among the immune cells involved, regulatory T cells (Tregs) have emerged as pivotal players in suppressing detrimental inflammation and facilitating tissue repair after MI.[7–9] Nevertheless, clinically viable strategies to safely and therapeutically enhance Treg function following MI remain elusive, representing a significant translational gap.

Suxiao Jiuxin Pill (SJP), a traditional Chinese medicine with established clinical use, presents a promising candidate to bridge this gap. It has been widely employed for the short-term relief of acute angina pectoris, effectively reducing attack frequency without significant side effects or drug resistance.[10,11] Notably, long-term administration of SJP significantly lowers the risk of MI recurrence, an effect strongly correlated with its capacity to alleviate myocardial fibrosis.[12] However, the mechanistic basis of these benefits, particularly beyond its known vasodilatory, metabolic regulatory, and cardiomyocyte-protective effects,[13–16] is incompletely understood.

Our study introduces a novel dimension to SJP's pharmacology: its role as a precise immunomodulator. We systematically investigate its previously unexplored capacity to target Treg-mediated repair post-MI. The novelty of our research is threefold: First, we shift the paradigm of SJP's action beyond its conventional roles to uncover a specific immunomodulatory function. Second, we demonstrate that SJP does not merely increase Treg numbers but functionally potentiates them. Third, we establish a causal role for Tregs in mediating SJP's cardioprotective effects through rigorous loss-of-function experiments. In summary, by repositioning a clinically available drug through the discovery of a new immunomodulatory mechanism, our work offers a promising and translatable therapeutic strategy to address the critical gap in post-MI Treg-targeted therapy.

Materials and Methods

Collection of SJP and MI Targets

The Traditional Chinese Medicine Systems Pharmacology Database and Analysis Platform (TCMSP, https://old.tcmsp-e.com/) was utilized to gather the chemical constituents of each individual herb in the SJP formula.[17] Potential targets of the complete chemical profiles of *Ligusticum chuanxiong* Hort. and *Borneolum syntheticum* were subsequently acquired. MI-associated targets were identified from the GSE232259 dataset (Mus musculus) (https://www.ncbi.nlm.nih.gov/geo/), which comprises 6 sham samples and 6 MI samples.[18] By applying the screening criteria ($p < 0.05$ and $|\log_2 FC| > 0.585$), retaining genes expressed in more than half of the samples, and conducting differential expression analysis using the three major R packages (DESeq2, edgeR, and limma), we identified a total of 6,369 differentially expressed genes. Subsequently, we selected the differential expression results from DESeq2 for further enrichment analysis. The results were visualized using ridgeplot, dotplot, and gseaplot2 to provide a comprehensive overview of the differentially expressed genes and their potential biological significance.

Kyoto Encyclopedia of Genes and Genomes (KEGG) Enrichment Analysis of SJP Against MI

To elucidate the mechanisms of action of the target sites, we intersected the SJP component targets with MI-related targets. The overlap was visualized using a Venn diagram through SangerBox Tools (http://sangerbox.com/).[19] Subsequently, we performed a KEGG enrichment analysis of the intersecting target proteins to more accurately understand their roles. The resulting common targets were input into the DAVID Functional Annotation Tool (https://david.ncifcrf.gov/), with the species "Mus musculus" selected. We downloaded the KEGG pathway module data and generated an enrichment bubble map using visualization tools from the website (https://www.bioinformatics.com.cn).[20] This approach allowed us to systematically explore the biological pathways associated with the identified targets.

Animals

Male C57BL/6 mice of specific pathogen free (SPF), aged 8–10 weeks and weighing 22–25 g, were purchased from Beijing Vital River Laboratory Animal Technology Co. Ltd and maintained at the Animal Center of Tianjin University of Traditional Chinese Medicine (Tianjin, China). All animals were kept under 22–25°C and a 12 h light/dark cycle with standard food pellets and free access to tap water. All animal care and experimental procedures were approved by the Animal Ethics Committee of Tianjin University of Traditional Chinese Medicine (IACUC Approval Number: TCM-LAEC2021031) and conducted in strict accordance with the national standard Guidelines for the Welfare and Ethics of Laboratory Animals (GB/T 35892–2018) of China.

Mouse Models and in vivo Protocols

The MI model was established by permanent ligation of the left anterior descending (LAD) coronary artery as described previously with modifications.[21] In brief, mice were anesthetized by an intraperitoneal injection of tribromoethanol (Avertin, 0.33mL/20g). Following the onset of anesthesia, mice were tracheally intubated and mechanically ventilated with the ventilator set to the following parameters: weight 0.05 kg, tidal volume 0.15 mL, respiratory rate 145 breaths per minute, and an inspiration-to-expiration ratio of 1:1. A left thoracotomy was performed at the fourth intercostal space, and the LAD was ligated with an 8–0 polypropylene suture. Successful MI was confirmed by immediate blanching of the anterior wall and ST-segment elevation on ECG. The sham group underwent identical surgery without LAD ligation. The SJP suspensions were prepared immediately before use by dissolving a 40 mg tablet in 5.12 mL of physiological saline. According to the dose conversion ratio between animals and humans, the dosage chosen for the study (SJP-M) is approximately equivalent to the human dosage (6.32 mg/kg/d). Mice were randomly divided into six groups: (1) Sham + Saline group, (2) MI + Saline group, (3) MI + SJP group (Zhongxin Pharmaceutical Group sixth TCM factory (Tianjin, China); National Drug Approval Number Z12020025; Product ID C14003000981) (39 mg/kg) (SJP-L) (4) MI + SJP group (78 mg/kg) (SJP-M), (5) MI + SJP group (156 mg/kg) (SJP-H), and (6) MI + Dapagliflozin group (1.5 mg/kg) (HY-10450, 99.96%, MedChemExpress, USA). The mice were daily treated with physiological saline, SJP-L, SJP-M, SJP-H, and dapagliflozin respectively for 14 days intragastrically. After MI surgery, mice were sacrificed. Hearts or blood were harvested for analysis.

Tregs Depletion in vivo

To achieve antibody-mediated depletion of Tregs, mice received a single intravenous injection (100 μg in 200 μL saline) of purified anti-mouse CD25 antibody (clone PC-61; Biolegend, cat. no. 102002) via the tail vein five days before MI. Control mice were administered an equivalent dose of purified Rat IgG1, λ isotype control antibody (Biolegend, cat. no. 401902) on the same schedule. The efficiency of Treg depletion was validated by flow cytometry, which revealed a near-complete ablation (approximately 100%) of $CD4^+CD25^+Foxp3^+$ cell frequency in the ischemic myocardium.[22]

Physiological Assessments of Left-Ventricular Function

Echocardiographic measurements were performed with a Vevo 2100™ high-resolution ultrasound biomicroscope and Vevo analysis software at days 3, 7 and 14. Mice were preanesthetized in an induction chamber using isoflurane and then transferred to a heated ECG platform for heart rate monitoring during the imaging procedure. The body temperature of

the animals was maintained at 37°C. During imaging, anesthesia was maintained with 1.0 vol% isoflurane delivered via a nosecone. Image acquisition was initiated with the transducer probe placed along the left sternal border to obtain the parasternal long-axis view, which displays both the apex and the outflow tract of the LV. An optimal parasternal long-axis projection was used for orientation. LV dimensions and contractility were measured from short-axis M-mode images for at least 3 consecutive cardiac cycles and then averaged. M-mode-based measurements included LV end-systolic (LVESV) and end-diastolic volumes (LVEDV), LV ejection fraction (LVEF), and LV fractional shortening (LVFS).[23]

Masson's Trichrome Staining

All hearts were harvested after the 14-day echocardiographic analysis, fixed with 4% paraformaldehyde, followed by ethanol dehydration and paraffin infiltration. Tissue blocks were sliced at a distance of 500 μm below the suture to produce 5 μm sections. Infarct size was evaluated on Masson's Trichrome staining. The fibrosis area was calculated as the ratio of the length of fibrotic area to the length of left-ventricular inner circumference with Image J software.

Histological Analysis

Hearts were obtained 5 days after operation and fixed with 4% paraformaldehyde. Tissues were dehydrated, embedded, and transversely sectioned into 5 μm pieces. These sections were stained by hematoxylin and eosin (HE) to detect cardiac tissue injury after ischemia.

Detection of Myocardial Enzymology

SJP was administered by oral gavage following the induction of MI. The first dose was given approximately 2 h after surgery, and serum biomarkers were assessed 24 h post-surgery, following two administrations of SJP. The extent of myocardial injury was evaluated by measuring serum levels of lactic dehydrogenase (LDH), creatine kinase (CK), creatine kinase isoenzyme (CK-MB), and cardiac troponin T (cTnT). Blood samples were collected 24 h after the surgical procedure. Levels of LDH, CK, and CK-MB were quantified using commercial colorimetric kits (Beijing Biosino, China) according to the manufacturer's protocols, with absorbance readings determined by a Hitachi 7020 automatic biochemical analyzer (Tokyo, Japan). Serum cTnT concentrations were measured using a commercially available ELISA kit (E-EL-M1801c, Elabscience®, China) in accordance with the manufacturer's instructions, and absorbance was read using a microplate reader (Biotek, USA).

Analysis of Cytokine Concentrations

IL-2 (E-EL-M0042c, Elabscience®, China), TNF-α (E-EL-M0049c, Elabscience®, China), IFN-γ (E-EL-M0048c, Elabscience®, China), and IL-17 (E-EL-M0047c, Elabscience®, China) were analysed by ELISA according to the manufacturer's instructions (Biotek, USA).

Quantitative RT-PCR Analysis

Total RNA was extracted from heart tissues using tissue homogenizers and TRIzol reagent (15596018, Invitrogen, USA) according to manufacturer's instructions. Transcript All-in-One-Strand cDNA Synthesis Kit (AT341, TransGen Biotech, Beijing, China) was used for the reverse transcription of RNA to cDNA. The mRNA levels were quantified by PerfectStart™ Green qPCR SuperMix (AQ101, TransGen Biotech, Beijing, China) in QuantStudio™ six Flex (Applied Biosystems, USA). Each sample was run in duplicate in a volume of 10 μL. Each group has more than three samples. The relative quantification of target gene expression was normalized to the expression of Gapdh. The relative gene expression was analysed by $2^{-\Delta\Delta CT}$ method. Data were expressed as fold change in mRNA level compared to a control group. The following mouse primers were used (Table 1).

Cell Isolation and Flow Cytometry

Mouse hearts were isolated for single cell preparation with atria and valves removed.[24] The heart tissues were minced in an ice box at 4 °C. The specimen was washed with a sterile DPBS solution to remove residual blood from the tissue. Then tissue fragments were digested with 2 mg/mL collagenase II (225 U/mg, LS004176, Worthington) and 1.2 U/mL Dispase II

Table 1 Primer Information for PCR in Mouse

Gene Name	Forward Primer	Reverse Primer
Gapdh	CAACGGGAAACCCATCACCA	ACGCCAGTAGACTCCACGACAT
Collagen III	ACGAGGTGACAAAGGTGAAACTGG	AGAACCTGGAGGACCTGGATTGC
CD206	*CAAGGAAGGTTGGCATTTGT*	*CCTTTCAGTCCTTTGCAAGC*
Lgals3	*TATGACCTGCCCTTGCCTGGAG*	*CTGTTTGCGTTGGGTTTCACTGTG*
Spp1	*AAGAGCGGTGAGTCTAAGGAGTCC*	*TGGCTGCCCTTTCCGTTGTTG*
Il1rl1	CAAGGTTCAGGGCACACAGGTC	GCCGTCACGATGTAGTTGGTTCC
Il33	TCAGGCGACGGTGTGGATGG	GGAGTAGTCCTTGTCGTTGGCATG
Inos	GGCAGCCTGTGAGACCTTTG	GCATTGGAAGTGAAGCGTTTC
Il10	GCTCTTACTGACTGGCATGAG	CGCAGCTCTAGGAGCATGTG
Ctla4	ACGGGACTGTACCTCTGCAA	TAAATCTGCGTCCCGTTGCC
Sparc	TGTCCTGGTCACCTTGTACGAGAG	TGGATCTTCTTCACACGCAGCTTC

(≥0.5 U/mg, D4693-1G, Sigma) in pre-heated 1640 medium (01–101-1A, Biological Industries, Israel) with HEPES buffer. Tissue was incubated at 37° C for 10 min with gentle rocking in gentleMACS C-tubes (Miltenyi Biotec, Germany), dissociated using "Heart 1" program of a gentleMACS Dissociator. Following incubation, tissue digestion buffer with tissue clusters was triturated by pipetting 12 times using a 5 mL pipette. Dishes were again incubated at 37° C and triturated twice more (30 min of total digestion time). All cell suspensions were placed into 15 mL tubes with 10 mL of neutralizing solution (DPBS+1% P.S.+2% heat inactivated FBS (04–121-1A, Biological Industries, Israel) +2mM EDTA) and filtered using a 40 μm cell strainer (BD Bioscience, USA) and centrifuged at 500 ×g for 10 min. Cell pellets were resuspended in 1% FBS/HBSS solution before staining with various antibodies and reagents for flow cytometry or FACS.

Heart mononuclear cells were stained with the following antibodies: CD45 (557235), CD11b (562605), F4/80 (565410), Ly6G (560600), CD8 (553030), CD62L (561919), CD44 (560569) (all from BD biosciences, USA); CD45 (103132), F4/80 (123112), Ly6G/Ly6C (108451), CD206 (141719), CD86 (105005), CD3 (100203), CD4 (100455), CD25 (101909) and ST2 (146609) (all from Biolegend, USA); CD4 (E-AB-F1097D, Elabscience, Wuhan, China). CompBeads Negative Control (51–90-9001291) and CompBeads Anti-Rat Ig (51–90-9001189) (BD biosciences, USA) were used to adjust compensation. IL-17A (506915, Biolegend) was performed using the Cell Activation Cocktail (423304, BioLegend). Fixation (420801, BioLegend) and Intracellular Staining Permeabilization Wash Buffer (10X) (421002, BioLegend) were used to fix and permeabilize cells. Intracellular labeling of Foxp3 (563101, BD biosciences) was performed using the BD Pharmingen™ TF Fix/Perm Buffer (4X) and TF Diluent Buffer and TF Perm/Wash Buffer (5X) (562574, BD biosciences). Viability was determined using the FVD (65–0868-14, 65–0864, eBioscience, San Diego, CA, USA) prior to fixation. Flow cytometry was performed on a FACSAriaIII instrument (BD Bioscience, USA) or NovoCyte Flow Cytometer (Agilent, China) and analyzed using FlowJo software or NovoExpress Software.

Naïve $CD4^+$ T Cell Isolation and Tregs Differentiation in vitro

After harvesting the spleens from 8-week-old male C57BL/6 mice, splenocytes were homogenized using a 70-μm cell strainer. Spleen Naïve $CD4^+$ T cell was sorted with a MojoSort™ Mouse CD4 Naïve T Cell Isolation Kit (480039, BioLegend, USA) according to the kit's instructions. Purity of isolated cells was then measured by flow cytometry. The purity of $CD4^+$ T cells was approximately 92.2%, the purity of naïve $CD4^+$ T cells ($CD4^+CD44^-CD62L^+$) was approximately 80.1%. For differentiation of Naïve $CD4^+$ T cell to Treg, approximately 3×10^5 naïve $CD4^+$ T cells were plated in 48-well plates in 0.5 mL complete RPMI 1640 medium and stimulated with plate-coated Ultra-LEAF™ Purified anti-mouse CD3ε antibody (5 μg/mL) (100339, Biolegend, USA), Ultra-LEAF™ Purified anti-mouse CD28

antibody (3 μg/mL) (102115, Biolegend, USA), recombinant mouse interleukin (IL)-2 (carrier-free) (5 ng/mL, 118 U/mL) (575402, Biolegend, USA), and recombinant human transforming growth factor (TGF)-β1 (carrier-free) (5 ng/mL) (781802, Biolegend, USA). The cells were incubated at 37 °C with 5% CO_2 for four days prior to analyzing the Treg purity. Treg purity ($CD4^+CD25^+Foxp3^+$) was then measured by flow cytometry.[25] The purity of Treg was approximately 90.7%. On day four, the half amount of culture medium of Treg was replaced with RPMI 1640 medium containing 1% FBS and 10 μM of the drug (Ligustrazine, Ferulic acid, Ligustilide, Senkyunolide A, Senkyunolide H, Senkyunolide I, Levistolide A, SJP-10, 20 μg/mL) (DST180302-032, DST180412-001, DST170315-007, DST200705-008, DST200117-182, DST200805-009, DST200602-001, Desite, Chengdu, China) (Table 2), with 3 wells for each group. After 24 h of intervention, Tregs were obtained for qRT-PCR analysis.

Molecular Docking

The mol2 structure files of Levistolide A, Ligustrazine, and Senkyunolide I were downloaded from the TCMSP platform. These structures were then subjected to energy minimization using Chem3D software, and the optimized structures were saved as mol2 files. Subsequently, the mol2 files were converted into pdb format using OpenBabel software. Meanwhile, the PDB structure of the ST2L protein was downloaded from the AlphaFold protein database. The three-dimensional structures of both the protein and the small molecules were uploaded to the CB-Dock2 website (https://cadd.labshare.cn/cb-dock2/php/example.php) for automated blind docking. The binding affinity between the ligand and receptor was evaluated based on energy matching, and the ligand with the highest binding affinity was selected for visualization.[28]

Table 2 The Levels of the Seven Main Components of SJP in the Heart[26,27]

Molecule Name	Structure	Heart
Ligustrazine		–
Levistolide A		≥5 ng/g
Senkyunolide A		≥120 ng/g
Ferulic acid		≥5 ng/g
Senkyunolide H		–
Senkyunolide I		≥120 ng/g
Ligustilide		≥120 ng/g

Statistical Analysis

Statistical analyses were performed using GraphPad Prism software (version 8.0, GraphPad Software, San Diego, CA, USA). Data are presented as mean ± SD. Differences between two groups were analyzed by an unpaired Student's *t*-test, while comparisons among three or more groups were analyzed by one-way ANOVA. A p-value of less than 0.05 was considered statistically significant.

The sample sizes for in vivo experiments were chosen based on established standards in the field of cardiovascular pharmacology and were consistent with those commonly reported in similar mechanistic studies in murine models of MI.

Results

SJP Improves Cardiac Function and Reduces Infarct Size Following MI

The MI model was successfully established by permanent ligation of the left anterior descending coronary artery. The experimental timeline, including assessment time points and biomarkers, is schematically illustrated in Figure 1A. Cardiac function was evaluated by echocardiography on days 3, 7, and 14 post-MI. Both SJP treatment and the positive control dapagliflozin significantly improved EF and FS compared to the saline group (Figure 1B and C). Histological analysis using Masson's trichrome staining revealed a significant reduction in the fibrotic area across all SJP-treated groups and the dapagliflozin group (Figure 1D and E). Furthermore, SJP treatment significantly upregulated *Collagen III* mRNA expression specifically within the infarcted area (Figure 1F). Analysis of serum biomarkers demonstrated that SJP-M treatment significantly attenuated the post-MI elevation of LDH, CK, CK-MB (Figure 1G–I), and cardiac troponin T (cTnT) (Figure 1J). Collectively, these results indicate that SJP improves cardiac function by enhancing the preservation and/or recovery of myocardial tissue, supporting its potential therapeutic efficacy in MI.

SJP May Improve Cardiac Function Through Regulating T Cell-Mediated Adaptive Immunity

Differentially expressed genes (DEGs) were derived from the GSE232259 dataset, comprising six sham-operated hearts and six post-MI hearts. These samples were initially visualized using principal component analysis (PCA). Differential expression analysis was then conducted using three major R packages (DESeq2, edgeR, and limma), resulting in the identification of a total of 6,369 differentially expressed genes. These genes were further visualized using heatmaps (Figure 2A). Subsequently, the differential expression results from DESeq2 were selected for further enrichment analysis. The results were visualized using ridgeplot, dotplot, and gseaplot2 to provide a comprehensive overview of the differentially expressed genes and their potential biological significance. The analysis revealed that the top three activated signaling pathways were epithelial-mesenchymal transition, inflammatory response, and allograft rejection, while the top three suppressed pathways were adipogenesis, oxidative phosphorylation, and fatty acid metabolism (Figure 2B–D). To elucidate the mechanisms of the target sites, we intersected the SJP component targets with MI-related targets. The overlap was visualized using a Venn diagram (Figure 2E). We then performed a KEGG enrichment analysis of the intersecting targets. The KEGG pathway enrichment analysis showed that SJP's effect on MI was significantly correlated with the TNF signaling pathway, Th17 cell differentiation, and NF-kappa B signaling pathway (Figure 2F). These findings indicate that inflammation activation is the dominant pathological event in left-ventricular MI. Most importantly, our analysis suggests that T cell-mediated adaptive immunity represents the principal pharmacological mechanism by which SJP rescues left-ventricular injury.

SJP Expands Tregs and Inhibits Th17 Cells in the Infarcted Area

The above results revealed that SJP may improve cardiac function through regulating T cell-mediated adaptive immunity. Therefore, we analyzed the T cells (including $CD4^+$T and $CD8^+$T) in the ischemic heart. Our data showed that, compared to the saline group, $CD4^+$ T cell percentages were significantly elevated in the SJP group post-MI (Figure 3A–C). $CD8^+$ T cells may be another type of cell that regulates the clearance of necrotic fragments in the infarcted area. However, our results showed that no differences were observed in the $CD8^+$ population at day 3 between groups (Figure 3D–F). Accordingly, we further examined the effects of SJP on the proportions of Treg and Th17 cells in the ischemic heart. Flow cytometry analysis revealed

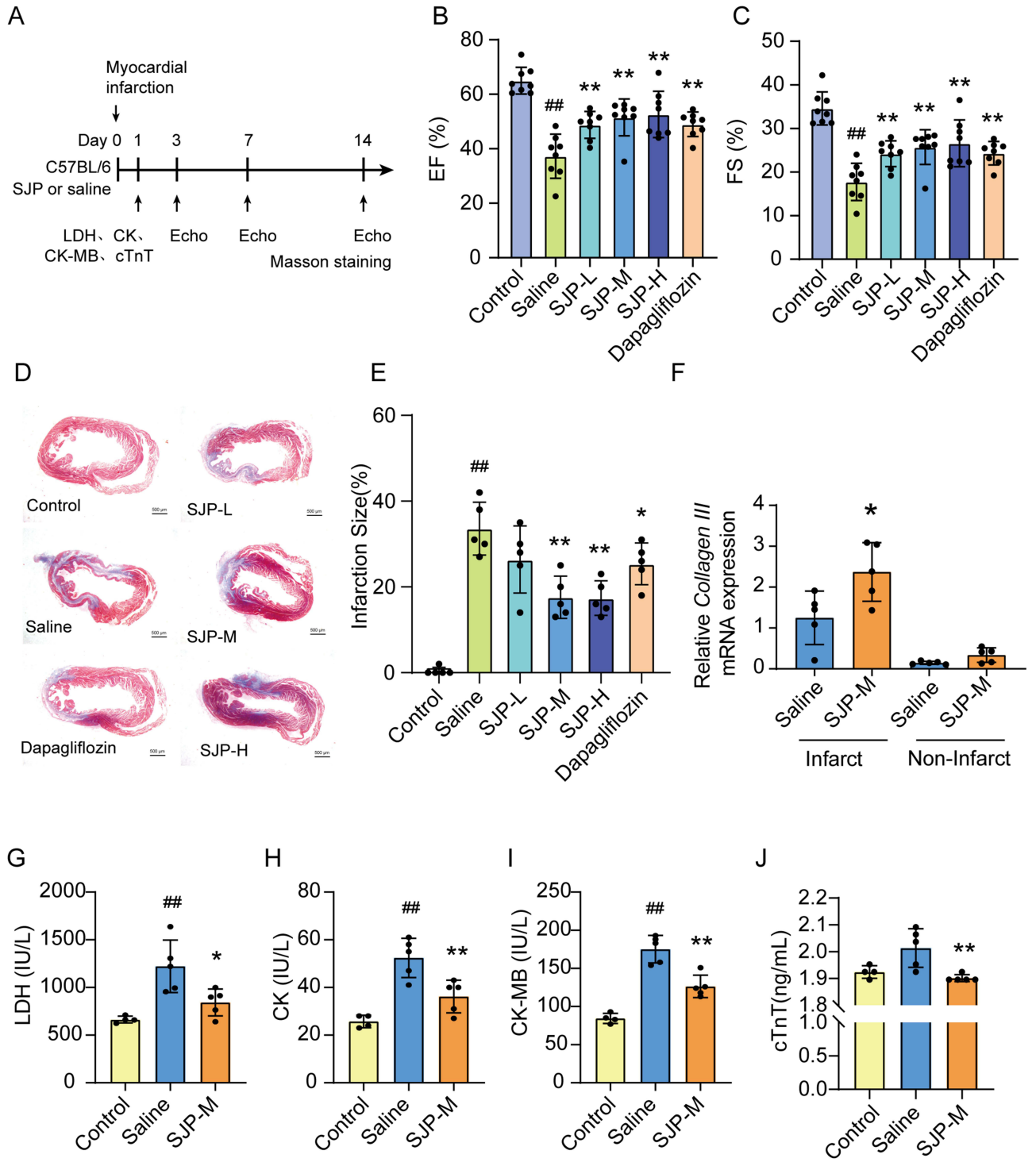

Figure 1 SJP improves cardiac function and reduces infarct size following MI. (**A**) Schematic protocol overview. Echo refers to echocardiogram. (**B** and **C**) SJP treatment enhances cardiac function following MI, as evidenced by improved EF and FS at 7 days post-MI (n = 8). Additional data for EF and FS at other time points following MI are presented in the supplementary Figure S1–S8. (**D**) Masson trichrome staining of heart sections at 14 days post-MI reveals fibrotic tissue, shown in blue-gray. (**E**) Quantitative analysis of fibrosis area at 14 days post-MI. Fibrosis is quantified as the ratio of the length of fibrotic tissue to the left ventricular circumference (n = 5). Scale bar = 500 μm. (**F**) qRT-PCR analysis of *Collagen III* mRNA in the infarcted and remote areas of the ischemic heart on day 14 post-MI (n = 5). (**G–I**) Changes in myocardial enzyme levels at 1-day post-MI. (**G**) LDH levels in each group. (**H**) CK levels in each group. (**I**) CK-MB levels in each group. (**J**) cTnT levels in each group at 1-day post-MI. Data are presented as mean ± SD. ##p < 0.01 vs control, *p < 0.05, **p < 0.01 vs saline.

https://doi.org/10.2147/JIR.S557620

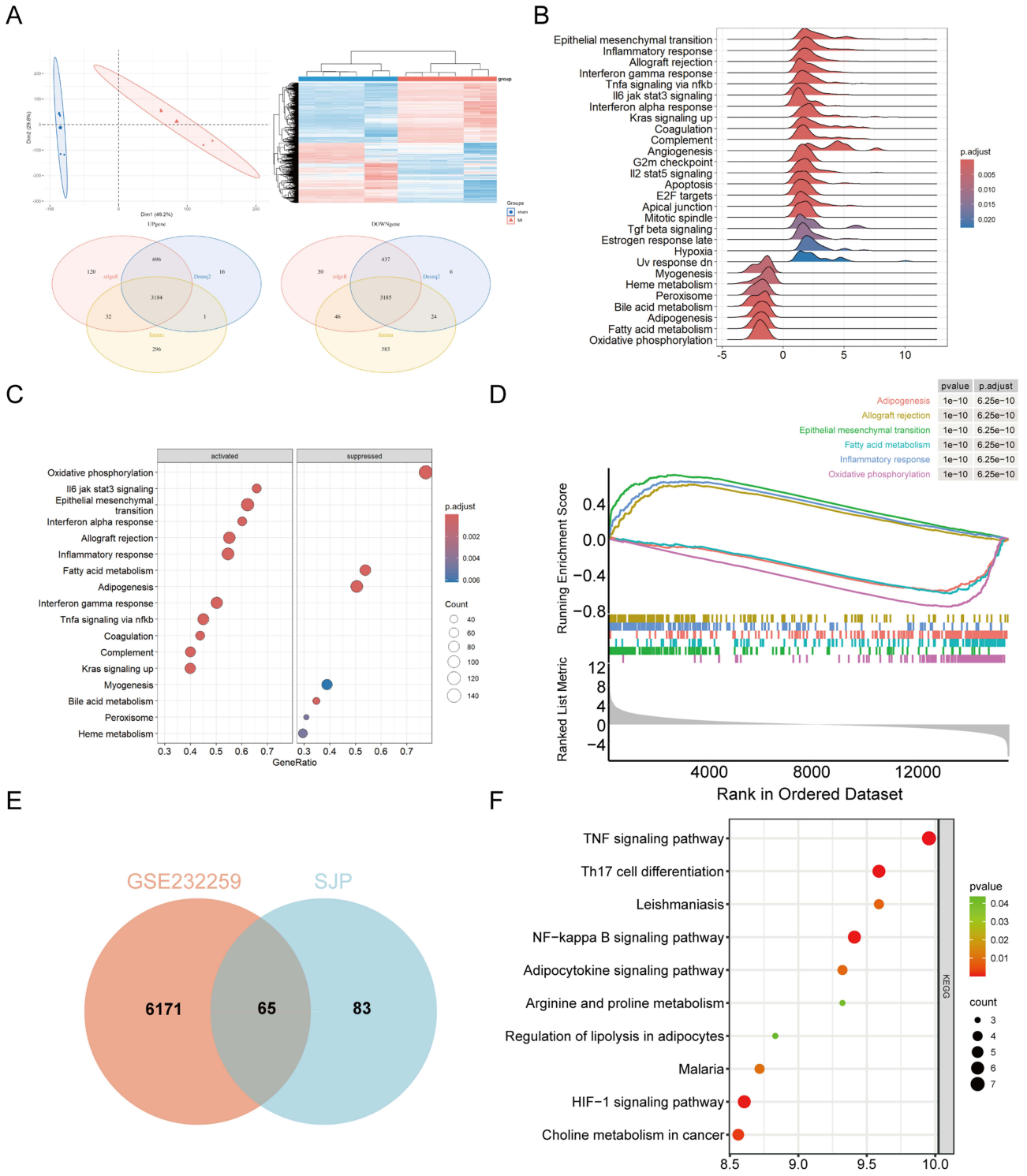

Figure 2 SJP may improve cardiac function through regulating T cell-mediated adaptive immunity. (**A**) DEGs were derived from the GSE232259 dataset, comprising six sham-operated hearts and six post-MI hearts. These samples were initially visualized using PCA. Differential expression analysis was then conducted using three major R packages (DESeq2, edgeR, and limma), resulting in the identification of a total of 6,369 differentially expressed genes. (**B** and **C**) The results were visualized using ridgeplot, and dotplot to provide a comprehensive overview of the differentially expressed genes and their potential biological significance. (**D**) The top three activated signaling pathways were epithelial-mesenchymal transition, inflammatory response, and allograft rejection, while the top three suppressed pathways were adipogenesis, oxidative phosphorylation, and fatty acid metabolism. (**E**) Intersected the SJP component targets with MI-related targets, and Venn diagrams were used to visualize these overlaps. (**F**) KEGG enrichment analysis on the intersecting targets.

https://doi.org/10.2147/JIR.S557620

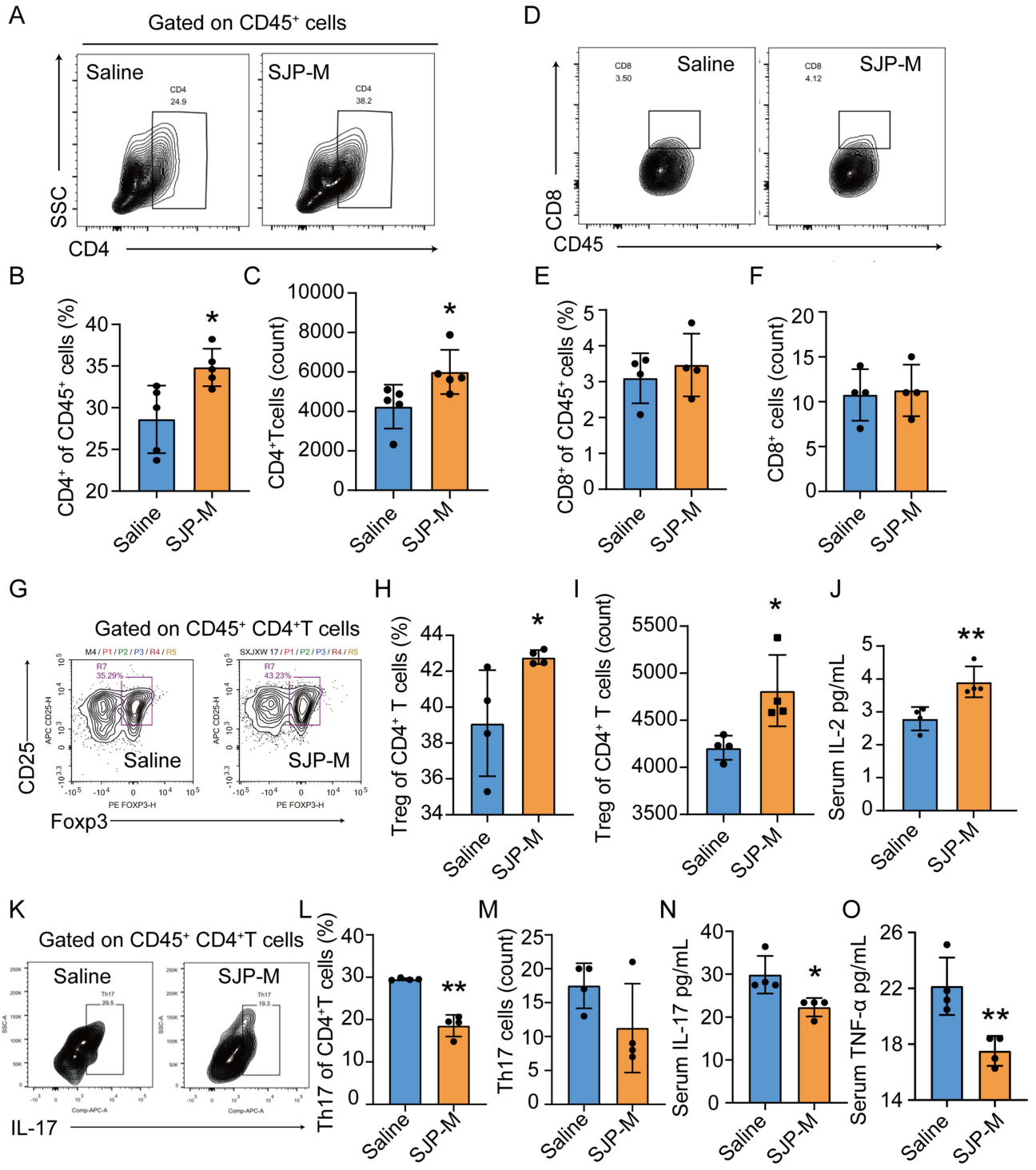

Figure 3 SJP expands Tregs and inhibits Th17 cells in the infarcted area. (**A**–**C**) Flow cytometry analysis of $CD4^+$ T cells post-MI (n = 5). (**D**–**F**) Flow cytometry analysis of $CD8^+$ T cells post-MI (n = 4). (**G**–**I**) Flow cytometry analysis of Tregs at day 5 post-MI (n = 4). (**J**) Quantification of IL-2 in serum post-MI in the presence of SJP or saline, detected by ELISA (n = 4). (**K**–**M**) Percentage of Th17 cells at day 5 post-MI (n = 4). (**N**) Quantification of IL-17 in serum post-MI in the presence of SJP or saline, detected by ELISA (n = 4). (**O**) Quantification of TNF-α in serum post-MI in the presence of SJP or saline, detected by ELISA (n = 4). Data are presented as mean ± SD. *$p < 0.05$, **$p < 0.01$ vs saline.

that SJP-M treatment significantly increased both the percentage (Figure 3G and H) and absolute count (Figure 3I) of Tregs ($CD4^+CD25^+Foxp3^+$) in the ischemic myocardium, accompanied by elevated serum IL-2 levels (Figure 3J). Concurrently, SJP-M reduced the proportion of Th17 cells ($CD4^+IL\text{-}17^+$) among $CD4^+$ T cells (Figure 3K and L) and decreased their absolute count (Figure 3M), while suppressing pro-inflammatory cytokines including IL-17 (Figure 3N) and TNF-α

https://doi.org/10.2147/JIR.S557620

(Figure 3O). These coordinated changes demonstrate that SJP-M promotes regulatory T cell responses while attenuating Th17-mediated inflammation in the post-infarction microenvironment. These findings suggest that SJP expands Tregs and inhibits Th17 cells in the infarcted area.

SJP Inhibits the Inflammatory Response in the Ischemic Heart

Our results showed that the proportion of neutrophils ($F4/80^{-}Gr1^{+}$) in SJP mice was lower than that in saline in the infarcted area (Figure 4A–C). On the 14th day after MI, the transcription of *CD206* in SJP group was significantly higher than that in saline group within the infarct but not remote area (Figure 4D). Intracellular galectin-3^{high} $CD206^{+}$ macrophages were involved in tissue repair through phagocytosis and fibrosis after MI. And osteopontin (OPN), almost exclusively produced by intracellular galectin-3^{high} $CD206^{+}$ macrophages, is an execution molecule for the clearance of dead cells by macrophages and the reparative fibrotic response.[29] Based on that, in the infarct and remote area, we investigated the transcription of *Lgals3* (encoding galectin-3), and *Spp1*(encoding OPN) post-MI. Our results showed that, *Lgals3* expression in the heart showed strong activation in the SJP group after MI (Figure 4E). The transcription of *Spp1* in SJP mice was higher than that in saline in the infarcted but not remote area post-MI (Figure 4F). These results were in-line with our hypothesis that SJP might reduce the infarcted area and improve cardiac function by inhibiting the inflammatory response in the ischemic heart following MI.

SJP and Its Active Ingredients Enhance the Function of Tregs

The transcription of *Il-10, Ctla-4*, and *Sparc* mRNA were analyzed in Tregs 1 day after drug intervention. The schematic protocol for Treg differentiation is shown in Figure 5A. Flow cytometric analysis demonstrated the purity of isolated $CD4^{+}$ T cells (92.2%) and naïve $CD4^{+}$ T cells ($CD4^{+}CD44^{-}CD62L^{+}$, 80.1%) (Figure 5B, upper panels). Following in vitro

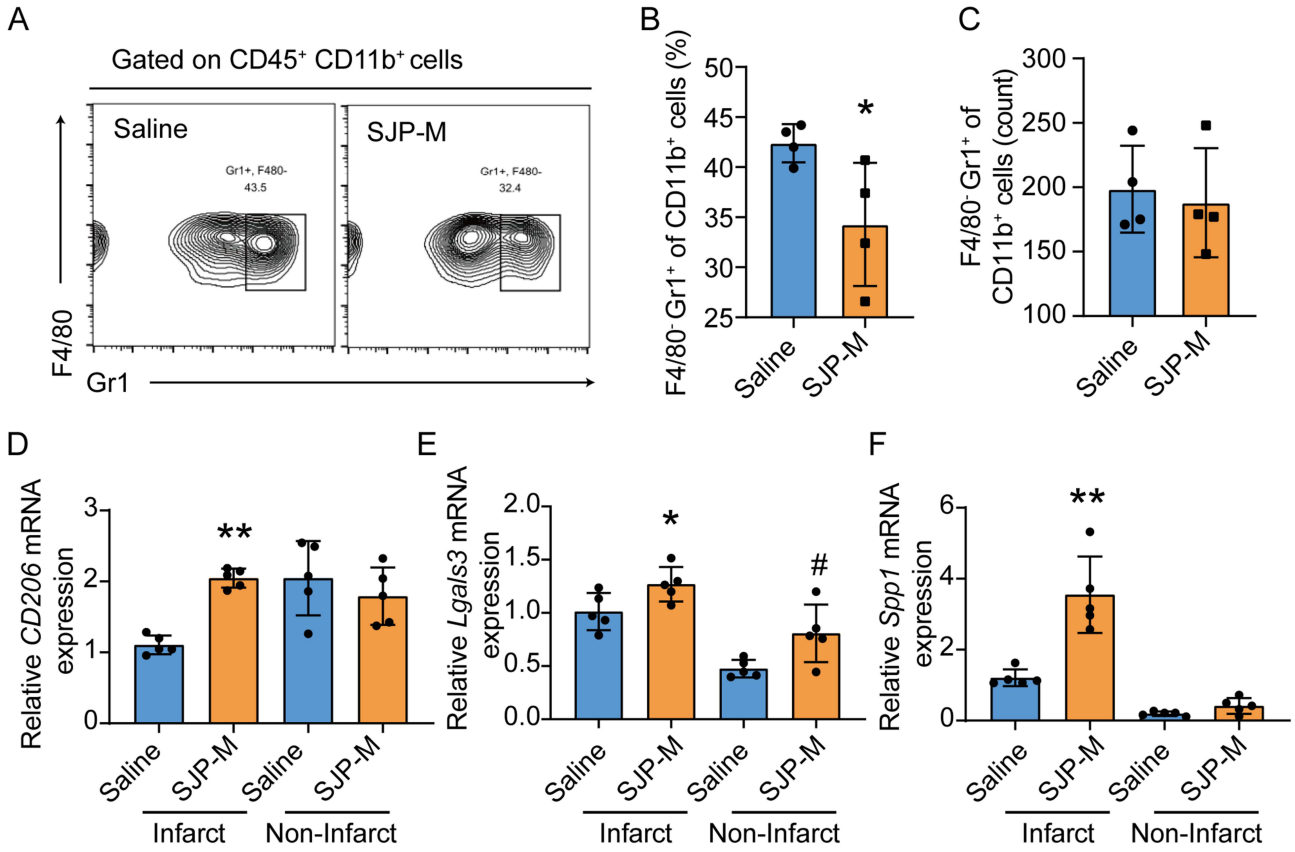

Figure 4 SJP inhibits the inflammatory response in the ischemic heart following MI. (**A**–**C**) Flow cytometry analysis of neutrophils post-MI (n = 4). (**D**–**F**) qRT-PCR analysis of *CD206, Lgals3* and *Spp1* mRNA in the infarct and remote area of the ischemic heart on day 14 post-MI (n = 5). Data are presented as mean ± SD. *$p < 0.05$ vs saline; *$p < 0.05$, **$p < 0.01$ vs infarct saline; #$p < 0.05$ vs non-infarct saline.

https://doi.org/10.2147/JIR.S557620

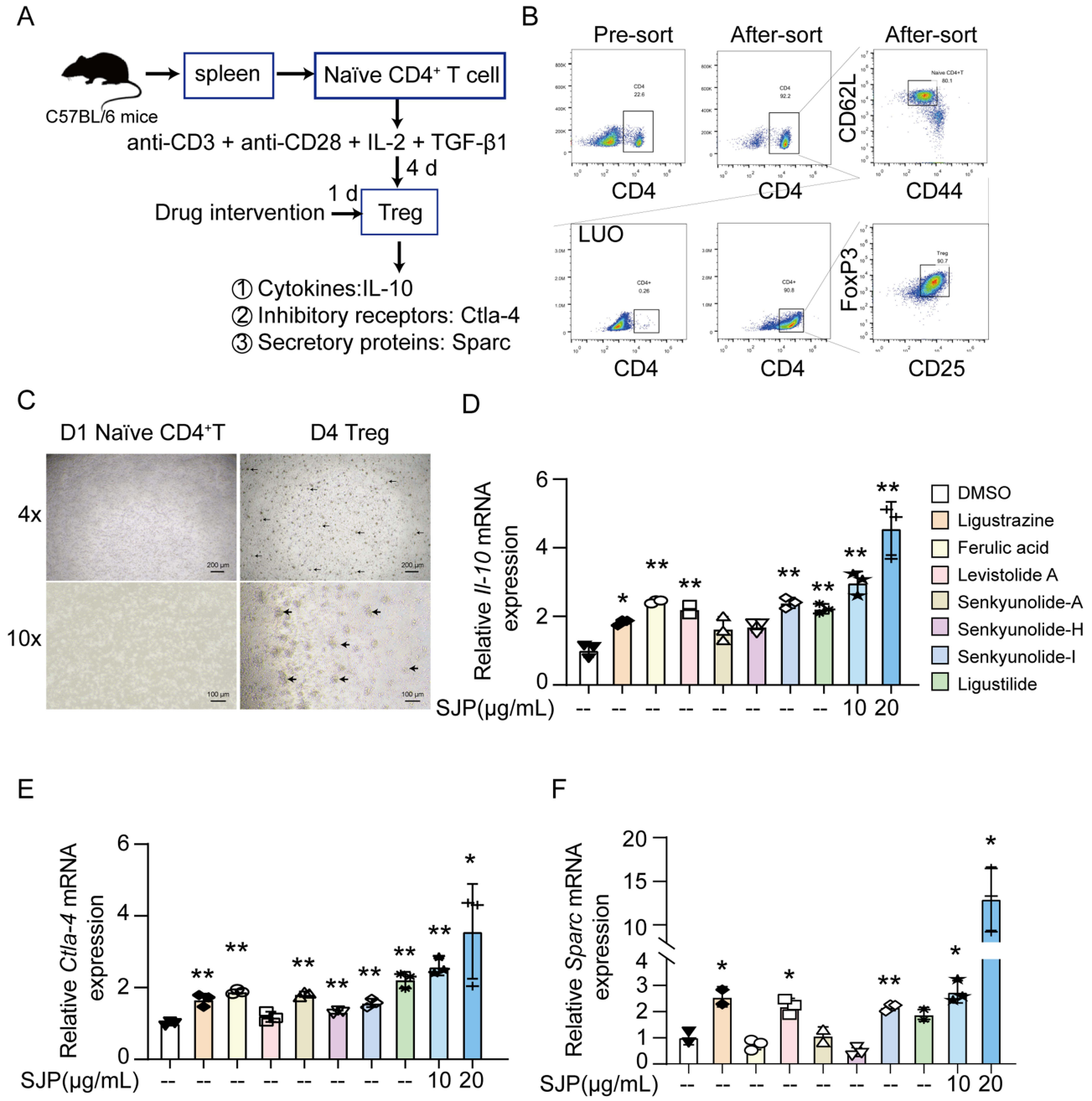

Figure 5 SJP and its active ingredients enhance the function of Tregs. (**A**) Schematic protocol for Treg differentiation. (**B**) Flow cytometry analysis of pre-sort $CD4^+$ cells, after-sort $CD4^+$ cells, after-sort naïve $CD4^+$ ($CD4^+CD62L^+CD44^-$) T cells, and Tregs ($CD4^+CD25^+Foxp3^+$). (**C**) Microscopic observation of naïve $CD4^+$ T cells sorted from the spleen on day 1 and 4-day Tregs induced from naïve $CD4^+$ T cells. The cell clustering observed is indicative of successful Treg differentiation, as indicated by the arrow. (**D**–**F**) qRT-PCR analysis of *Il-10, Ctla-4*, and *Sparc* mRNA in Tregs (n = 3). Data are presented as mean ± SD. *$p < 0.05$, **$p < 0.01$ vs DMSO.

differentiation, Treg purity ($CD4^+CD25^+Foxp3^+$) reached 90.7% (Figure 5B, lower panels). The successful differentiation was further morphologically confirmed by microscopic observation of characteristic Treg clustering (Figure 5C). In vitro results showed that SJP and its main active ingredients, including ligustrazine, ferulic acid, levistolide A, senkyunolide I, and ligustilide upregulated the transcription of *Il-10* mRNA in Tregs (Figure 5D). Ligustrazine, ferulic acid, senkyunolide A, senkyunolide H, senkyunolide I, and ligustilide upregulated the transcription of *Ctla-4* mRNA in Tregs (Figure 5E). Additionally, Ligustrazine, levistolide A, and senkyunolide I enhanced the transcription of *Sparc* mRNA in Tregs (Figure 5F). Taken together, these data support that SJP and its active ingredients enhance the function of Tregs.

SJP Expands Tregs in the Infarcted Area by Activating the ST2L Signaling

Previous studies have demonstrated that the IL-33/ST2L axis is essential for maintaining cardiac Treg populations.[8] We initially examined the transcriptional levels of IL-33 and ST2L in cardiac tissue. The results indicated that IL-33 was significantly upregulated post-MI, but SJP did not further alter its abundance (Figure 6A), suggesting that SJP acts on the receptor rather than the ligand. Compared with the saline group, SJP significantly upregulated the transcription of Il1rl1 (encoding ST2L) mRNA in infarcted areas (Figure 6B). Using flow cytometry, we examined the expression of ST2L in cardiac cells and found that ST2L is predominantly expressed on $CD45^+CD4^+$ T cells in the ischemic heart (Figure 6C–E). Notably, SJP had no effect on ST2L expression on $CD4^+$ T cells. However, compared with the saline group, SJP upregulated ST2L on $CD4^+Foxp3^+$ Tregs (Figure 6F–H). To identify which SJP constituents directly engage ST2L, we performed molecular docking of key ingredients. Levistolide A and senkyunolide I were identified as high-affinity binders to ST2L (Figure 6I–K). With binding energies lower than –5 kcal mol^{-1}, these compounds are predicted to stabilize the ST2L receptor complex and trigger downstream signaling that culminates in Foxp3 induction and Treg polarization (Figure 6L). Collectively, our data demonstrate that SJP-derived levistolide A and senkyunolide I bind to ST2L on Tregs, activate the ST2L signaling pathway, and expand Tregs in the infarcted area.

SJP Suppresses Inflammatory Cell Infiltration in the Ischemic Heart Through Treg Cell-Dependent Mechanisms Post-MI

Tregs are essential for immune homeostasis and restrain the progression of inflammatory diseases.[30] To determine whether SJP mitigates myocardial ischemic injury by expanding the Treg pool after MI, we administered an anti-CD25 antibody via tail-vein injection to deplete Tregs. Flow cytometry confirmed that both the frequency and absolute number of $CD4^+Foxp3^+$ Tregs in the ischemic myocardium were effectively abolished by day 5 post-MI (Figure 7A–C). Histological analysis revealed that SJP markedly attenuated myocardial damage and reduced inflammatory cell infiltration compared with saline controls. In striking contrast, Treg depletion-whether given saline or SJP-resulted in exacerbated tissue injury and dense leukocyte infiltrates (Figure 7D).

We next examined the impact of SJP on innate immune cells following Treg ablation. Flow cytometry showed that SJP significantly lowered the proportion of neutrophils ($CD11b^+Ly6G^+$) in the infarcted area relative to the saline group on day 5 post-MI; this protective effect was reversed when Tregs were depleted (Figure 8A–C). Similarly, SJP diminished pro-inflammatory macrophages ($F4/80^+CD86^+$) in the infarct, yet this reduction persisted despite Treg loss (Figure 8D–F). However, Treg depletion uncovered a marked SJP-induced up-regulation of *Inos* mRNA-indicative of heightened pro-inflammatory macrophage activity (Figure 8G). Conversely, expression of the reparative macrophage genes *Lgals3* (encoding galectin-3) and *Spp1* (encoding osteopontin), as well as the anti-inflammatory cytokine *Il-10* produced by both reparative macrophages and Tregs, were significantly down-regulated after Treg removal (Figure 8H–J). Collectively, these data demonstrate that SJP dampens neutrophil and pro-inflammatory macrophage infiltration while promoting a reparative macrophage phenotype in the ischemic heart, and these effects are critically dependent on Tregs.

Discussion

MI initiates a complex inflammatory response that is pivotal for tissue repair but also for the progression of adverse remodeling. Despite the life-saving benefits of reperfusion therapies, a critical unmet need remains for treatments that can effectively modulate the post-MI immune landscape to foster repair. Our study demonstrates that the traditional Chinese medicine formula SJP ameliorates post-MI cardiac injury primarily by enhancing the function and regulation of Tregs via the ST2L signaling pathway, thereby unveiling a sophisticated multi-component immunomodulatory strategy.

Our findings necessitate a systematic comparison with the existing research landscape. Positioning within SJP research, while earlier studies established SJP's efficacy in angina relief and its anti-fibrotic effect,[13–16] our work unveils its previously unexplored, precise immunomodulatory role, clarifying the progression from known clinical effects to a novel mechanistic discovery. Contextualizing our mechanistic findings within Treg biology and MI repair, the identification of the ST2L pathway as a key mechanism aligns with the recognized importance of the IL-33/ST2 axis in Treg-mediated cardio-protection. However, our research delineates how a complex botanical formula orchestrates this axis through multi-component synergy, moving beyond single-agent approaches.

https://doi.org/10.2147/JIR.S557620

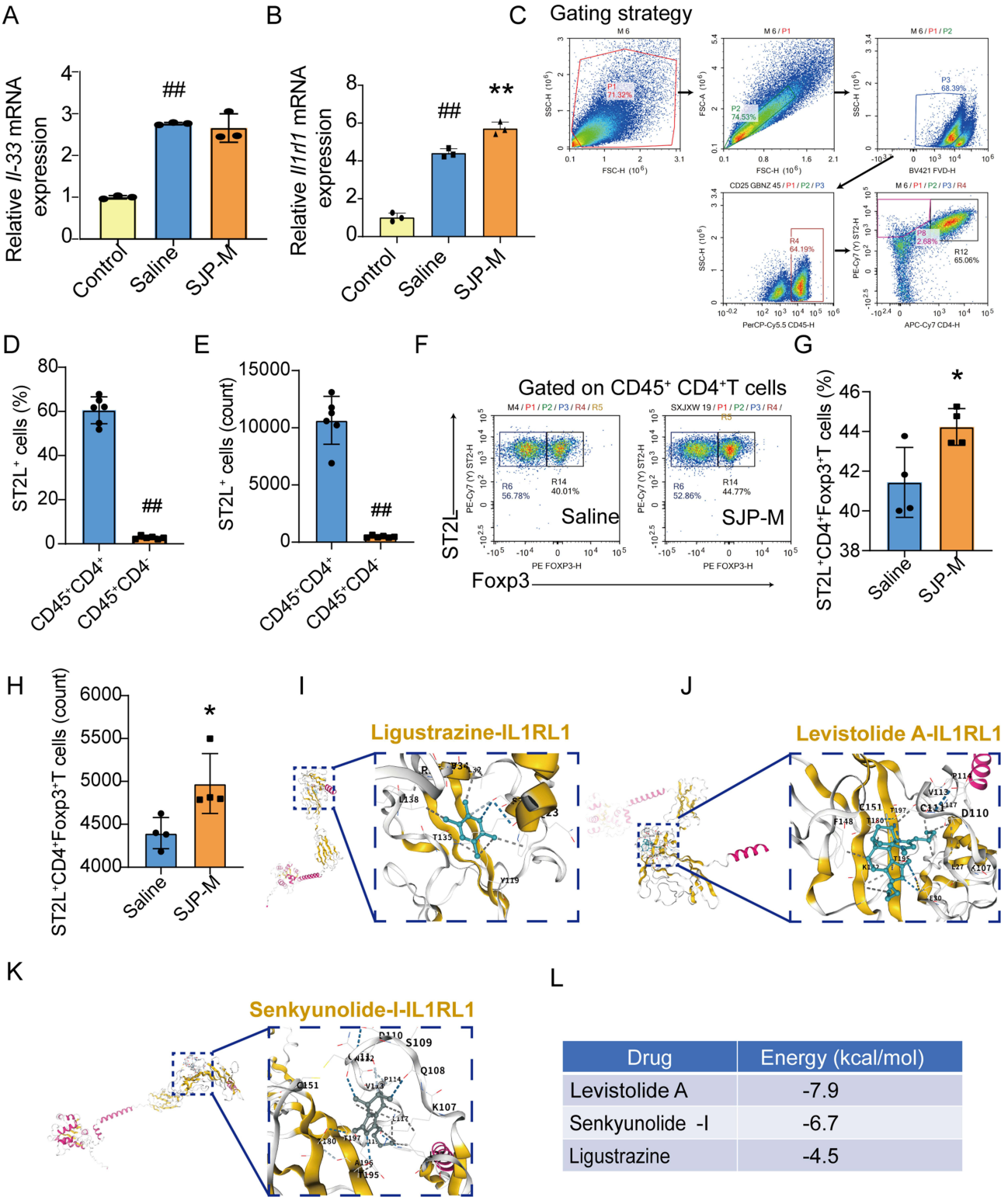

Drug	Energy (kcal/mol)
Levistolide A	-7.9
Senkyunolide -I	-6.7
Ligustrazine	-4.5

Figure 6 SJP expands Tregs in the infarcted area by activating the ST2L signaling. (**A**) Effect of SJP on *Il-33* mRNA expression in infarcted areas following MI (n = 3). (**B**) Effect of SJP on *Il1rl1* mRNA expression in infarcted areas following MI (n = 3). (**C-E**) Flow cytometry analysis of $CD45^+CD4^+ST2L^+$ cells (n = 6). (**F–H**) Flow cytometry analysis of $Foxp3^+ST2L^+$ cells at day 5 post-MI (n = 4). (**I-K**) Molecular docking of SJP core components and target genes. (**I**) ST2L (IL1RL1) and ligustrazine. (**J**) ST2L (IL1RL1) and levistolide A. (**K**) ST2L (IL1RL1) and senkyunolide I. (**L**) The binding energy between the small molecule and IL1RL1. Data are presented as mean ± SD. *$p < 0.05$, **$p < 0.01$ vs saline; ##$p < 0.01$ vs Control; ##$p < 0.01$ vs $CD45^+CD4^+$.

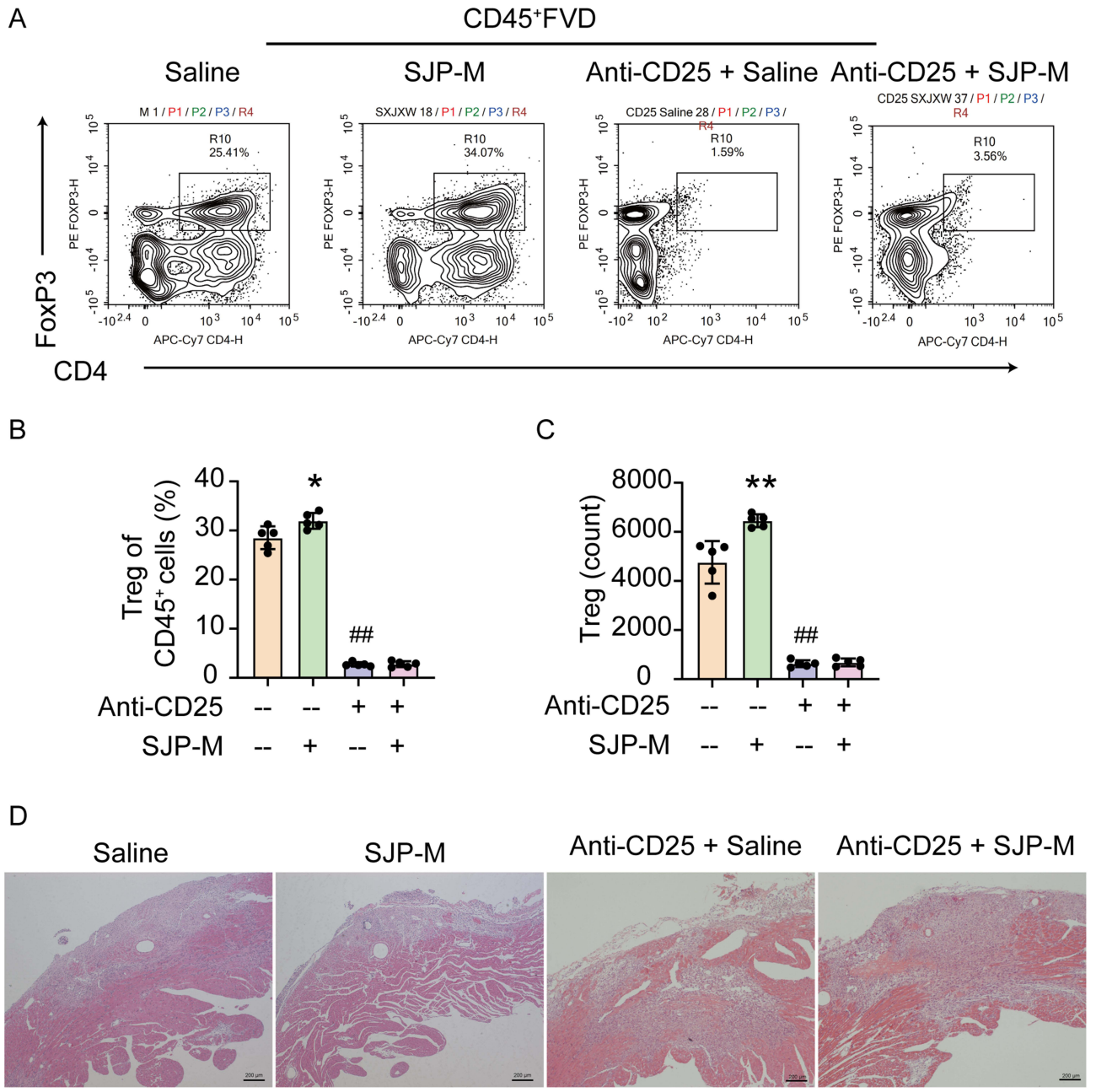

Figure 7 SJP suppresses myocardial ischemia injury through Treg cell-dependent mechanisms post-MI. (**A**–**C**) Flow cytometry was performed to confirm the successful depletion of Tregs following anti-CD25 treatment. Treg levels, including the percentage of Foxp3$^+$ cells within total CD45$^+$ cells and the number of Tregs in the ischemic heart, were determined (n = 5). (**D**) H&E staining was used to assess myocardial injury. Data are presented as mean ± SD. *p < 0.05, **p < 0.01 vs saline; ##p < 0.01 vs Anti-CD25 + saline.

The significance of our data is further highlighted by its unique therapeutic positioning. Unlike conventional Treg-targeted therapies such as low-dose IL-2 or adoptive Treg transfer—which face challenges regarding a narrow therapeutic window, off-target effects, and practical delivery—SJP demonstrates a capacity to orchestrate a balanced and self-limiting immune response.[8,31–36] It focuses more on "functional regulation" and microenvironment remodeling than on mere "numerical expansion", potentially offering a more suitable approach for the chronic phase of post-MI healing. Compared to broad-spectrum immunosuppressants like corticosteroids, which indiscriminately suppress immunity, SJP exhibits a more nuanced and safer profile, achieving a favorable shift in the Treg/Th17 balance without causing broad immune paralysis.[37,38] This coordinated, multi-component action highlights a potential key advantage of multi-target botanical drugs over single-target agents.

https://doi.org/10.2147/JIR.S557620

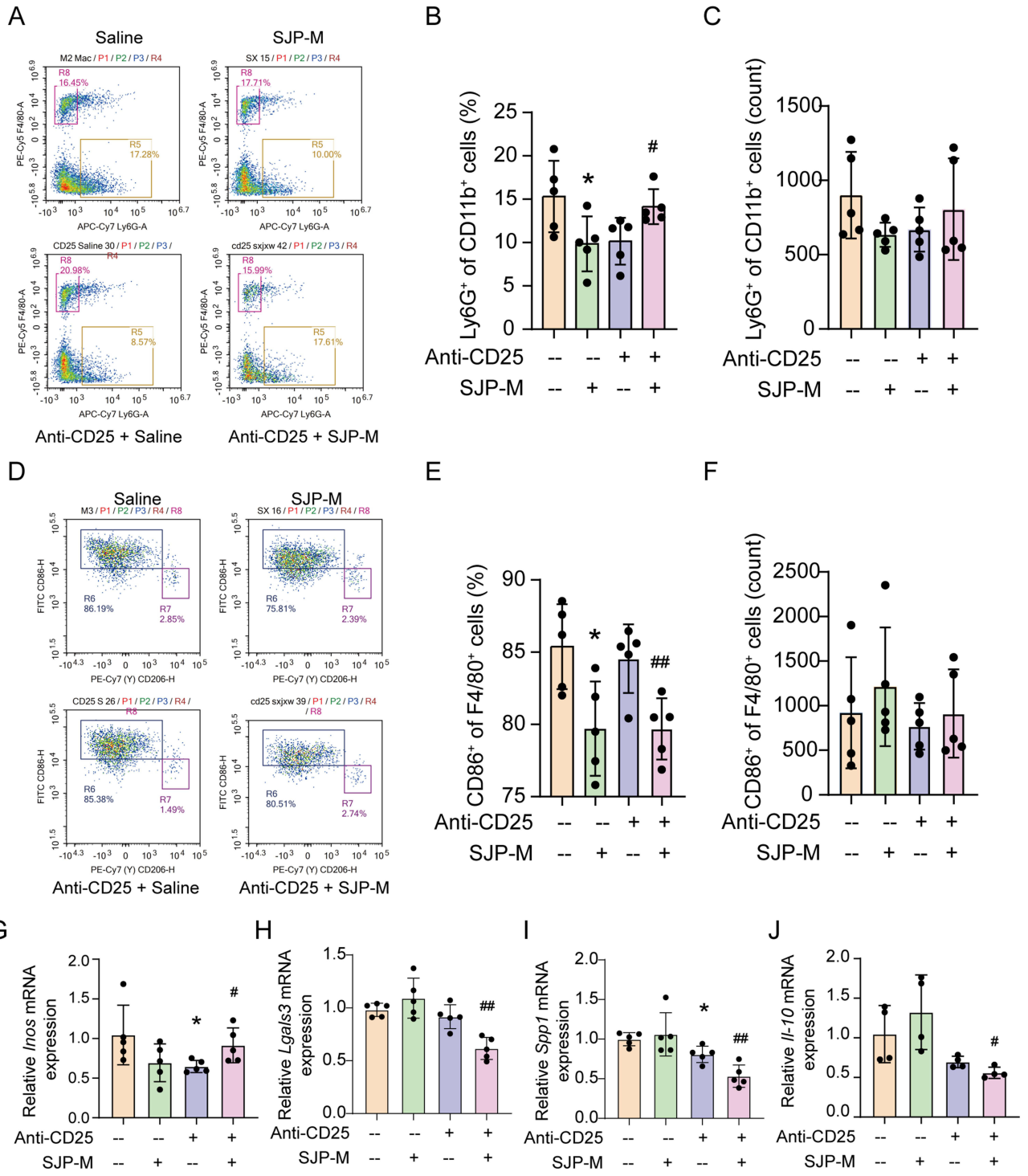

Figure 8 SJP suppresses inflammatory cell infiltration in the ischemic heart through Treg cell-dependent mechanisms post-MI. (**A**–**C**) After Treg depletion, flow cytometry analysis was conducted to assess the proportion of neutrophils ($CD11b^+Ly6G^+$) on day 5 post-MI. (**D**–**F**) After Treg depletion, flow cytometry analysis was conducted to assess the proportion of pro-inflammatory macrophages ($F4/80^+CD86^+$) on day 5 post-MI (n = 5). (**G**–**J**) qRT-PCR analysis was performed to measure *iNOS*, *Lgals3*, *Spp1*, *Il10* mRNA expression in the infarcted area of the ischemic heart on day 5 post-MI (n = 5). Data are presented as mean ± SD. *$p < 0.05$ vs saline; #$p < 0.05$, ##$p < 0.01$ vs Anti-CD25 + saline.

The safety profile of SJP is underpinned by decades of real-world clinical application in managing cardiovascular diseases, providing a level of assurance distinct from newer biologics associated with specific side effects like vascular leak syndrome, or targeted small molecules with black-box warnings.[12,39,40]

However, the promising therapeutic potential of targeting the ST2L pathway, as validated by our study, comes with complexities. Previous studies have demonstrated that recombinant IL-33 can directly enhance the immunosuppressive function of Tregs via ST2L, promote Treg expansion, and alleviate disease severity in models of arthritis and transplantation tolerance.[41] Furthermore, in a lupus nephritis model, combined use of an ST2L pathway agonist (eg, recombinant IL-33) with low-dose IL-2 was shown to expand and stabilize the Treg compartment more effectively than IL-33 alone,[42] although this strategy has not yet advanced to clinical translation. In the context of cardiovascular diseases, the IL-33/ST2L pathway has been implicated in post-MI cardiac repair.[43,44] Our study, by elucidating that SJP exerts cardioprotective effects via the ST2L/Foxp3 signaling axis, further supports the therapeutic potential of targeting this pathway for immunomodulation after MI. Yet, the same pathway can drive pathology in conditions like allergic rhinitis.[45] Therefore, clarifying the tissue-specific characteristics of ST2L-targeted therapies—such as functional and responsiveness differences between cardiac Tregs and systemic Tregs—is crucial for minimizing off-target risks and facilitating clinical translation. Given the complexity of immune regulatory networks, we propose that future research should focus on exploring combination immunotherapy approaches, coupled with precisely defined therapeutic time windows for immune intervention, to provide a theoretical foundation and practical pathway for optimizing treatment strategies.

Despite promising preclinical results, several limitations and translational barriers must be acknowledged. We note that the primary mechanistic insights were derived from a mouse model, and validation in human pathophysiology is required. As a multi-component botanical drug, defining the comprehensive pharmacokinetic profiles and potential synergistic interactions among its constituents presents a major challenge. Ensuring batch-to-batch consistency is fundamental for reproducible clinical outcomes. Before advancing to human trials, identifying the most suitable patient subgroup and sensitive biomarkers for immunomonitoring is crucial steps. Currently, the clinical application of SJP is established for angina, but to our knowledge, no large-scale trials have been initiated for its specific application in post-MI immunomodulation as investigated here.

Looking forward, for future applicability, we suggest investigating SJP in more complex disease models (eg, with aging or comorbidities) to enhance clinical predictive value. The exciting potential for drug repurposing should be explored in future clinical trials. Beyond SJP itself, our study validates the ST2L pathway as a therapeutically relevant target. Future studies should investigate whether this cardioprotective paradigm can be replicated by other ST2L-targeted agents (eg, recombinant IL-33 or specific ST2L agonists) and focus on combination strategies to provide a foundation for optimizing treatment.[46]

Conclusion

This study elucidates that SJP promotes post-MI cardiac repair through a sophisticated immunomodulatory mechanism. SJP expands the cardiac Treg population and remodels the immune microenvironment towards a reparative state. Crucially, it augments the immunosuppressive function of Tregs by activating the ST2L/Foxp3 signaling pathway, with senkyunolide I and levistolide A identified as the primary active constituents. These findings not only provide a solid experimental and mechanistic foundation for the long-term clinical application of SJP but also highlight the therapeutic potential of finely-tuned, multi-component immunomodulation in the treatment of ischemic heart disease.

Abbreviations

SJP, Suxiao Jiuxin Pill; MI, myocardial infarction; ST2L, Interleukin 1 receptor-like 1 (membrane-bound isoform, IL-33 receptor); IL-33, Interleukin-33; LVEF, left-ventricular ejection fraction; LVFS, left-ventricular fractional shortening; LDH, lactic dehydrogenase; CK, creatine kinase; CK-MB, creatine kinase isoenzyme; cTnT, cardiac troponin T; FCM, Flow Cytometry; Treg, regulatory T cells; ELISA, enzyme-linked immunosorbent assay; HE, haematoxylin and eosin; Il-10, Interleukin-10; Ctla-4, Cytotoxic T Lymphocyte-Associated Protein 4; Sparc, secreted acidic cysteine rich glycoprotein; iNOS, Inducible Nitric Oxide Synthase.

Author Contributions

All authors made a significant contribution to the work reported, whether that is in the conception, study design, execution, acquisition of data, analysis and interpretation, or in all these areas; took part in drafting, revising or critically

reviewing the article; gave final approval of the version to be published; have agreed on the journal to which the article has been submitted; and agree to be accountable for all aspects of the work.

Funding

This research was funded by the National Natural Science Foundation of China (Grant Number: 82274135); the Key Laboratory Project of the Shaanxi Provincial Department of Education (Grant Number: 23JS053); Research Fund for the Doctoral Program of Xi'an Medical University (Grant Number: 2023BS18).

Disclosure

The authors report no conflicts of interest in this work.

References

1. Chaitman BR, Alexander KP, Cyr DD, et al. Myocardial infarction in the ISCHEMIA trial: impact of different definitions on incidence, prognosis, and treatment comparisons. *Circulation*. 2021;143(8):790–804. doi:10.1161/CIRCULATIONAHA.120.047987
2. Safiri S, Karamzad N, Singh K, et al. Burden of ischemic heart disease and its attributable risk factors in 204 countries and territories, 1990–2019. *Eur J Prev Cardiol*. 2022;29(2):420–431. doi:10.1093/eurjpc/zwab213
3. Mackman N, Bergmeier W, Stouffer GA, Weitz JI. Therapeutic strategies for thrombosis: new targets and approaches. *Nat Rev Drug Discov*. 2020;19(5):333–352. doi:10.1038/s41573-020-0061-0
4. Doenst T, Haverich A, Serruys P, et al. PCI and CABG for treating stable coronary artery disease. *J Am Coll Cardiol*. 2019;73(8):964–976. doi:10.1016/j.jacc.2018.11.053
5. Zhang Y, Cai Z, Shen Y, et al. Hydrogel-load exosomes derived from dendritic cells improve cardiac function via Treg cells and the polarization of macrophages following myocardial infarction. *J Nanobiotechnol*. 2021;19(1):271. doi:10.1186/s12951-021-01016-x
6. Soni SS, D'Elia AM, Rodell CB. Control of the post-infarct immune microenvironment through biotherapeutic and biomaterial-based approaches. *Drug Deliv Transl Res*. 2023;13(7):1983–2014. doi:10.1007/s13346-023-01290-2
7. Weirather J, Hofmann UDW, Beyersdorf N, et al. Foxp3 + CD4 + T cells improve healing after myocardial infarction by modulating monocyte/macrophage differentiation. *Circ Res*. 2014;115(1):55–67. doi:10.1161/CIRCRESAHA.115.303895
8. Xia N, Lu Y, Gu M, et al. A unique population of regulatory T cells in heart potentiates cardiac protection from myocardial infarction. *Circulation*. 2020;142(20):1956–1973. doi:10.1161/CIRCULATIONAHA.120.046789
9. Tang -T-T, Yuan J, Zhu Z-F, et al. Regulatory T cells ameliorate cardiac remodeling after myocardial infarction. *Basic Res Cardiol*. 2012;107(1):232. doi:10.1007/s00395-011-0232-6
10. Ren L, Wang J, Feng L, Wang S, Li J. Efficacy of Suxiao Jiuxin Pill on coronary heart disease: a meta-analysis of randomized controlled trials. *Evid Based Complement Alternat Med*. 2018;2018:9745804. doi:10.1155/2018/9745804
11. Shen Z, Chen T, Deng B, et al. Effects on Suxiao Jiuxin Pills in the treatment of patients with acute coronary syndrome undergoing early percutaneous coronary intervention: a multicenter randomized double-blind placebo-controlled trial. *J Altern Complement Med*. 2020;26(11):1055–1063. doi:10.1089/acm.2020.0014
12. Wu Z, Wang X, Zhang M, Liu Z, Ruan X, He Z. Chinese experts consensus on Suxiao Jiuxin Pill in treating of coronary heart disease. *Chin J Integr Med Cardio*. 2019;3265–3267. doi:10.12102/j.issn.1672-1349.2019.21.001
13. Lei W, Ni J, Xia X, Jiang M, Bai G. Searching for synergistic calcium antagonists and novel therapeutic regimens for coronary heart disease therapy from a traditional Chinese medicine, Suxiao Jiuxin Pill. *J Chromatogr B Analyt Technol Biomed Life Sci*. 2018;1092:220–227. doi:10.1016/j.jchromb.2018.06.015
14. Ruan X, Chen T, Wang X, Li Y. Suxiao Jiuxin Pill protects cardiomyocytes against mitochondrial injury and alters gene expression during ischemic injury. *Exp Ther Med*. 2017;14(4):3523–3532. doi:10.3892/etm.2017.4964
15. Ruan X-F, Ju C-W, Shen Y, et al. Suxiao Jiuxin pill promotes exosome secretion from mouse cardiac mesenchymal stem cells in vitro. *Acta Pharmacol Sin*. 2018;39(4):569–578. doi:10.1038/aps.2018.19
16. Wu G, Zhong J, Chen L, et al. Effects of the Suxiao Jiuxin pill on acute myocardial infarction assessed by comprehensive metabolomics. *Phytomedicine*. 2020;77:153291. doi:10.1016/j.phymed.2020.153291
17. Zhou W, Wang Y. A network-based analysis of the types of coronary artery disease from traditional Chinese medicine perspective: potential for therapeutics and drug discovery. *J Ethnopharmacol*. 2014;151(1):66–77. doi:10.1016/j.jep.2013.11.007
18. Kou S, Lu Z, Deng D, et al. Activation of imprinted gene PW1 promotes cardiac fibrosis after ischemic injury. *Circulation*. 2025;151(9):623–639. doi:10.1161/CIRCULATIONAHA.124.070738
19. Chen D, Xu L, Xing H, et al. Sangerbox 2: enhanced functionalities and update for a comprehensive clinical bioinformatics data analysis platform. *Imeta*. 2024;3(5):e238. doi:10.1002/imt2.238
20. Tang D, Chen M, Huang X, et al. SRplot: a free online platform for data visualization and graphing. *PLoS One*. 2023;18(11):e0294236. doi:10.1371/journal.pone.0294236
21. Wu M, Zhou J, Cheng M, et al. E2F1 suppresses cardiac neovascularization by down-regulating VEGF and PlGF expression. *Cardiovasc Res*. 2014;104(3):412–422. doi:10.1093/cvr/cvu222
22. Solomon I, Amann M, Goubier A, et al. CD25-treg-depleting antibodies preserving IL-2 signaling on effector T cells enhance effector activation and antitumor immunity. *Nat Cancer*. 2020;1(12):1153–1166. doi:10.1038/s43018-020-00133-0
23. Rusinkevich V, Huang Y, Chen Z-Y, et al. Temporal dynamics of immune response following prolonged myocardial ischemia/reperfusion with and without cyclosporine A. *Acta Pharmacol Sin*. 2019;40(9):1168–1183. doi:10.1038/s41401-018-0197-1

24. Pinto AR, Chandran A, Rosenthal NA, Godwin JW. Isolation and analysis of single cells from the mouse heart. *J Immunol Methods*. 2013;393(1–2):74–80. doi:10.1016/j.jim.2013.03.012
25. Lopez-Pastrana J, Shao Y, Chernaya V, Wang H, Yang X-F. Epigenetic enzymes are the therapeutic targets for CD4+CD25+/highFoxp3+ regulatory T cells. *Transl Res*. 2015;165(1):221–240. doi:10.1016/j.trsl.2014.08.001
26. Li S, Zhan J, Wang Y, et al. Suxiao Jiuxin Pill attenuates acute myocardial ischemia via regulation of coronary artery tone. *Front Pharmacol*. 2023;14:1104243. doi:10.3389/fphar.2023.1104243
27. Shang Y, Zhu Y, Zhou S, et al. A UPLC-MS/MS coupled with GC-MS method for quantification of twenty-one chemical ingredients from Suxiao Jiuxin pill in multiple tissue of rat and its application to tissue distribution study. *J Pharm Biomed Anal*. 2025;252:116461. doi:10.1016/j.jpba.2024.116461
28. Liu Y, Yang X, Gan J, Chen S, Xiao Z-X, Cao Y. CB-Dock2: improved protein–ligand blind docking by integrating cavity detection, docking and homologous template fitting. *Nucleic Acids Res*. 2022;50(W1):W159–W164. doi:10.1093/nar/gkac394
29. Shirakawa K, Endo J, Kataoka M, et al. IL (Interleukin)-10–STAT3–galectin-3 axis is essential for osteopontin-producing reparative macrophage polarization after myocardial infarction. *Circulation*. 2018;138(18):2021–2035. doi:10.1161/CIRCULATIONAHA.118.035047
30. Delgobo M, Weiss E, Ashour D, et al. Myocardial milieu favors local differentiation of regulatory T cells. *Circ Res*. 2023;132(5):565–582. doi:10.1161/CIRCRESAHA.122.322183
31. Kim HT, Koreth J, Whangbo J, et al. Organ-specific response after low-dose interleukin-2 therapy for steroid-refractory chronic graft-versus-host disease. *Blood Adv*. 2022;6(15):4392–4402. doi:10.1182/bloodadvances.2022007773
32. Niu Y, Lei S, Liu C, et al. Adoptive transfer of TregIL-33 cells ameliorates acute graft-versus-host disease by regulating the HPGD/PGE2 pathway. *Int Immunopharmacol*. 2026;168(Pt 1):115700. doi:10.1016/j.intimp.2025.115700
33. Hirakawa M, Matos TR, Liu H, et al. Low-dose IL-2 selectively activates subsets of CD4+ Tregs and NK cells. *JCI Insight*. 2016;1(18):e89278. doi:10.1172/jci.insight.89278
34. Dong S, Hiam-Galvez KJ, Mowery CT, et al. The effect of low-dose IL-2 and treg adoptive cell therapy in patients with type 1 diabetes. *JCI Insight*. 2021;6(18). doi:10.1172/jci.insight.147474
35. Hippen KL, Hefazi M, Larson JH, Blazar BR. Emerging translational strategies and challenges for enhancing regulatory T cell therapy for graft-versus-host disease. *Front Immunol*. 2022;13:926550. doi:10.3389/fimmu.2022.926550
36. Zeng Z, Yu K, Chen L, Li W, Xiao H, Huang Z. Interleukin-2/anti-interleukin-2 immune complex attenuates cardiac remodeling after myocardial infarction through expansion of regulatory T cells. *J Immunol Res*. 2016;2016:8493767. doi:10.1155/2016/8493767
37. Zhou H, Zhao X, Zhang R, et al. Low-dose IL-2 mitigates glucocorticoid-induced treg impairment and promotes improvement of SLE. *Signal Transduct Target Ther*. 2023;8(1):141. doi:10.1038/s41392-023-01350-6
38. Cangemi R, Falcone M, Taliani G, et al. Corticosteroid use and incident myocardial infarction in adults hospitalized for community-acquired pneumonia. *Ann Am Thorac Soc*. 2019;16(1):91–98. doi:10.1513/AnnalsATS.201806-419OC
39. Thom AK, Fraker DL, Norton JA. IL-1 receptor antagonist (IL-1ra) augments IL-2-induced pulmonary vascular leak. *J Surg Res*. 1993;54(4):336–341. doi:10.1006/jsre.1993.1054
40. Wollenberg A, Ikeda M, Chu C-Y, et al. Longer-term safety and efficacy of baricitinib for atopic dermatitis in pediatric patients 2 to <18 years old: a randomized clinical trial of extended treatment to 3.6 years. *J DermatolTreat*. 2024;35(1):2411834. doi:10.1080/09546634.2024.2411834
41. Biton J, Khaleghparast Athari S, Thiolat A, et al. In vivo expansion of activated Foxp3+ regulatory T cells and establishment of a type 2 immune response upon il-33 treatment protect against experimental arthritis. *J Immunol*. 2016;197(5):1708–1719. doi:10.4049/jimmunol.1502124
42. Stremska ME, Jose S, Sabapathy V, et al. IL233, A novel IL-2 and IL-33 hybrid cytokine, ameliorates renal injury. *J Am Soc Nephrol*. 2017;28(9):2681–2693. doi:10.1681/ASN.2016121272
43. Thanikachalam PV, Ramamurthy S, Mallapu P, et al. Modulation of IL-33/ST2 signaling as a potential new therapeutic target for cardiovascular diseases. *Cytokine Growth Factor Rev*. 2023;71-72:94–104. doi:10.1016/j.cytogfr.2023.06.003
44. Garbern JC, Williams J, Kristl AC, et al. Dysregulation of IL-33/ST2 signaling and myocardial periarteriolar fibrosis. *J Mol Cell Cardiol*. 2019;128:179–186. doi:10.1016/j.yjmcc.2019.01.018
45. Liu G, Liu F. Advances of IL-33/ST2 signaling pathway in allergic rhinitis. *Lin Chuang Er Bi Yan Hou Tou Jing Wai Ke Za Zhi*. 2020;34(6):565–568. doi:10.13201/j.issn.2096-7993.2020.06.020
46. Yu J, Li Y, Hu J, Wang Y. Interleukin-33 induces angiogenesis after myocardial infarction via AKT/eNOS signaling pathway. *Int Immunopharmacol*. 2024;143(Pt 3):113433. doi:10.1016/j.intimp.2024.113433